

## A Study of DNA Tube Formation Mechanisms Using 4-, 8-, and 12-Helix DNA Nanostructures

Yonggang Ke, Yan Liu, Junping Zhang, and Hao Yan\*

Contribution from the Department of Chemistry and Biochemistry, and The Biodesign Institute, Arizona State University, Tempe, Arizona 85287

Received November 30, 2005; E-mail: hao.yan@asu.edu

**Abstract:** This paper describes the design and characterization of a new family of rectangular-shaped DNA nanostructures (DNA tiles) containing 4, 8, and 12 helices. The self-assembled morphologies of the three tiles were also investigated. The motivation for designing this set of DNA nanostructures originated from the desire to produce DNA lattices containing periodic cavities of programmable dimensions and to investigate the mechanism of DNA tube formation. Nine assembly scenarios have been investigated through the combination of the three different tiles and three sticky end association strategies. Imaging by atomic force microscopy (AFM) revealed self-assembled structures with varied cavity sizes, lattice morphologies, and orientations. Six samples show only tube formation, two samples show both 2D lattices ( $>2 \mu\text{m}$ ) and tubes, and one sample shows only 2D lattices without tubes. We found that a lower tile dimensional anisotropy, weaker connection, and corrugated design favor the large 2D array formation, while the opposite (higher tile anisotropy, stronger connection, and uncorrugated design) favors tube formation. We discuss these observations in terms of an energy balance at equilibrium and the kinetic competition between diffusion-limited lateral lattice growth versus fluctuation of the lattice to form tubes at an early stage of the assembly. The DNA nanostructures and their self-assembly demonstrated herein not only provide a new repertoire of scaffolds to template the organization of nanoscale materials, but may also provide useful information for investigating other self-assembly systems.

### Introduction

In recent years, a number of research groups have begun developing nanofabrication methods based on DNA self-assembly.<sup>1–12</sup> This begins with the self-assembly of single-stranded DNA molecules (generally 10–120 nucleotides) into branched motifs known as tiles. DNA tiles carry single-stranded overhangs or sticky ends, which are designed to bind complementary sticky ends of other tiles, allowing the tiles to self-assemble into ordered lattices. Self-assembled DNA 2D arrays

comprising billions to trillions of DNA tiles have already been demonstrated.<sup>13</sup> The ability to program the self-assembly of DNA provides a powerful platform to organize other nanocomponents into functional architectures.<sup>14–21</sup>

In earlier designs of self-assembled DNA tiling arrays, people frequently observed several micrometer long ribbons (100–500 nm wide) or tubes ( $\sim 20$ –100 nm in diameter). Examples of such tiling systems include different versions of double crossover (DX) tiles,<sup>22–24</sup> triple crossover (TX) tiles,<sup>25</sup> and  $4 \times 4$  cross-shaped tiles.<sup>4</sup> The DNA tubes have been proposed as potential

- (1) Winfree, E.; Liu, F.; Wenzler, L. A.; Seeman, N. C. *Nature* **1998**, *394*, 539–544.
- (2) LaBean, T. H.; Yan, H.; Kopatsch, J.; Liu, F.; Winfree, E.; Reif, J. H.; Seeman, N. C. *J. Am. Chem. Soc.* **2000**, *122*, 1848–1860.
- (3) Mao, C.; Sun, W.; Seeman, N. C. *J. Am. Chem. Soc.* **1999**, *121*, 5437–5443.
- (4) Yan, H.; Park, S. H.; Finkelstein, G.; Reif, J. H.; LaBean, T. H. *Science* **2003**, *301*, 1882–1884.
- (5) Liu, D.; Wang, M.; Deng, Z.; Walulu, R.; Mao, C. *J. Am. Chem. Soc.* **2004**, *126*, 2324–2325.
- (6) Ding, B.; Sha, R.; Seeman, N. C. *J. Am. Chem. Soc.* **2004**, *126*, 10230–10231.
- (7) Rothmund, P. W. K.; Papadakis, N.; Winfree, E. *PLoS Biol.* **2004**, *2*, 2041–2053.
- (8) Malo, J.; Mitchell, J. C.; Venien-Bryan, C.; Harris, J. R.; Wille, H.; Sherratt, D. J.; Turberfield, A. J. *Angew. Chem., Int. Ed.* **2005**, *44*, 3057–3061.
- (9) Chelyapov, N.; Brun, Y.; Gopalkrishnan, M.; Reishus, D.; Shaw, B.; Adleman, L. *J. Am. Chem. Soc.* **2004**, *126*, 13924–13925.
- (10) Feng, L.; Park, S. H.; Reif, J. H.; Yan, H. *Angew. Chem., Int. Ed.* **2003**, *42*, 4342–4346.
- (11) Mathieu, F.; Liao, S.; Kopatsch, J.; Wang, T.; Mao, C.; Seeman, N. C. *Nano Lett.* **2005**, *5*, 661–665.
- (12) Park, S. H.; Barish, R.; Li, H.; Reif, J. H.; Finkelstein, G.; Yan, H.; LaBean, T. H. *Nano Lett.* **2005**, *5*, 693–696.
- (13) He, Y.; Chen, Y.; Liu, H.; Ribbe, A. E.; Mao, C. *J. Am. Chem. Soc.* **2005**, *127*, 12202–12203.
- (14) Loweth, C. J.; et al. *Angew. Chem., Int. Ed.* **1999**, *38*, 1808–1812.
- (15) Xiao, S.; et al. *J. Nanopart. Res.* **2002**, *4*, 313.
- (16) Le, J. D.; Pinto, Y.; Seeman, N. C.; Musier-Forsyth, K.; Taton, T. A.; Kiehl, R. A. *Nano Lett.* **2004**, *4*, 2343.
- (17) Deng, Z.; Tian, Y.; Lee, S.; Ribbe, A. E.; Mao, C. *Angew. Chem., Int. Ed.* **2005**, *44*, 3582–3585.
- (18) Claridge, S. A.; et al. *Chem. Mater.* **2005**, *17*, 1628–1635.
- (19) Li, H.; Park, S. H.; Reif, J. H.; LaBean, T. H.; Yan, H. *J. Am. Chem. Soc.* **2004**, *126*, 418–419.
- (20) Niemeyer, C. M.; Koehler, J.; Wuerdemann, C. *ChemBioChem* **2002**, *3*, 242.
- (21) Liu, Y.; Lin, C.; Li, H.; Yan, H. *Angew. Chem., Int. Ed.* **2005**, *44*, 4333–4338.
- (22) Rothmund, P.; Ekani-Nkodo, A.; Papadakis, N.; Kumar, A.; Fyngenson, D.; Winfree, E. *J. Am. Chem. Soc.* **2004**, *126*, 16344–16352.
- (23) Ekani-Nkodo, A.; Kumar, A.; Fyngenson, D. K. *Phys. Rev. Lett.* **2004**, *93*, 1–4.
- (24) Mitchell, J. C.; Harris, J. R.; Malo, J.; Bath, J.; Turberfield, A. J. *J. Am. Chem. Soc.* **2004**, *126*, 16342–14363.
- (25) Liu, D.; Park, S. H.; Reif, J. H.; LaBean, T. H. *Proc. Natl. Acad. Sci. U.S.A.* **2004**, *101*, 717–722.

structural materials. Because of their extreme stiffness, they may be used as models for microtubules.<sup>22</sup> It was also suggested that DNA tubes could be used as size-specific reaction vessels.<sup>22</sup> On the other hand, a flat 2D lattice is desirable for applications such as molecular lithography mask production.<sup>26</sup> However, it is important to determine the factors affecting the growth of DNA tiles into either tubes or flat lattices. By understanding this, one could tune the design parameters to obtain the desired lattice morphology.

Two independent studies specifically investigated the mechanism of DNA tube formation<sup>22,24</sup> from two similar DX tiles, a DAE-E<sup>22</sup> tile and a DAE-O<sup>24</sup> tile. Here, DAE-E or DAE-O means each tile contains a double crossover, antiparallel orientation of the strands through the crossover, even number of half-turns for intramolecular distance between crossovers, and even or odd number of half-turns for intermolecular distance between crossovers. The integral number of half-turns is required for planar assembly. Self-assembly studies using the above two tiles as unit building blocks both lead to observation of DNA tubes.<sup>22,24</sup> The DNA tubes created from the two different tiles show some interesting differences: in the DAE-E case, the tubes all have narrow circumference distribution and the tube axis is parallel to the tile helix axis (except when DNA hairpins were added).<sup>22</sup> In the DAE-O case, there is a relatively wide size distribution of the tubes and a wide orientation distribution of the tube axis with respect to the tile axis.<sup>24</sup>

The DAE-E and DAE-O tiles used in the two studies share many similarities in shape and size but differ by the intermolecular distance between crossovers: even number of half helical turns for a DAE-E tile or odd number of half helical turns for a DAE-O tile. When the tiles are self-assembled into arrays, the neighboring tiles show the same face on the same side of the array for the DAE-E tiles but show alternating faces for the DAE-O tiles. When examined more closely, in the case of DAE-E tiles studied by Rothmund et al.,<sup>22</sup> the two complementary single-stranded sticky ends for the neighboring tiles are linked to the strands that do not participate in the intermolecular crossover points. Because there are an even number of half-turns for intermolecular distance between crossovers, the angle between the planes of two neighboring tiles is equal to that between the major and minor grooves, that is,  $\sim 150 \pm 10^\circ$  (see more details and schemes in ref 22). It was understood that this inter-tile angle led to the closing of a patch of tile array to form a tube. The tube circumference can be predicted from the inter-tile angle to be 4–8 tiles, which is consistent with the narrow tubes observed.<sup>22</sup> For the DAE-O tiles studied by Turberfield and co-workers,<sup>24</sup> the two complementary single-stranded sticky ends for the neighboring tiles are linked to the strands that participate in the intermolecular crossover points. Therefore, there is a  $180^\circ$  angle between the two neighboring tiles, and the angle between two tiles separated by one tile is  $0^\circ$ . The tube formation using DAE-O tiles was understood as an energetically driven phenomenon.<sup>24</sup> Closing up a patch of tiles into a tube reduces the free energy of the tile array by satisfying all inter-tile bonds except those at the ends of the tube, although it also requires a strain energy penalty that bends the tile array. By balancing the energy change, an upper limit of the flexural rigidity (bending modulus) perpendicular to the long axis of the tile,  $D_{\perp}$ , was estimated to be  $< 3$

$\times 10^{-20}$  J, based on the narrowest tubes observed (radius  $\sim 20$  nm) and the bond energy ( $\sim 10$  kcal/mol for two pairs of 6-base sticky ends). Another estimate based on the twisting modulus of DNA double helix gives a  $D_{\perp} \sim 6 \times 10^{-21}$  J (ref 24, Supporting Information). From the persistence length ( $\sim 50$  nm) of double helical DNA, the flexural rigidity along the tile axis,  $D_{\parallel}$ , is estimated to be  $\sim 1 \times 10^{-19}$  J, which is at least 3 times larger than  $D_{\perp}$ . Therefore, one can explain why the tubes mostly wrap around the tile axis.

We agree with both the geometry and the energy arguments. However, when large 2D lattices instead of DNA tubes are formed, which have been observed previously and here in this study, some other factors must be considered in the model. It has been pointed out that the tube diameter is likely determined by a nonequilibrium process,<sup>24</sup> because once the tube has closed, an activation barrier prevents further lateral growth. It can be imagined that the first event of the tile array closing into a ring will guide the tile array to grow only along both ends into a longer tube, which should keep the diameter of the initial ring. The earlier the tube closes, the narrower the tube diameter will be. However, no upper limit of the tube diameter is given.<sup>24</sup> We think that under some kinetic conditions one might be able to prevent tube formation to obtain a large 2D array.

In this work, we designed a new family of rectangular-shaped DNA tiles with variable dimensional anisotropy. Three different tile systems and three different strategies of association between the tiles were used. We examined and discussed the role of tile dimensional anisotropy, the relative orientation of the tiles, and the strength of the tile connectivity in the tube formation.

## Design

The 4-, 8-, and 12-helix DNA tile complexes (4-HT, 8-HT, and 12-HT) were designed to form planar rectangular-shaped tiles (Figure 1A–C). Within each tile, the DNA helices are arranged parallel to their neighboring helices and are joined together side by side in a plane with two crossovers running from one helix to its neighboring helix(es). Each pair of neighboring helices in the complex has a geometry similar to that of a DAE double crossover molecule.<sup>1</sup> As illustrated at the bottom of Figure 1A–C, there is a dihedral angle of  $120^\circ$  when viewed along the helical axes. The design principle here is similar to a previously reported six-helix bundle DNA complex.<sup>11</sup> The difference is that we used 7 nucleotide base pairs between the two closest crossovers of neighboring helices, and the crossovers run back and forth alternatively so that eventually all of the crossovers sit on one plane to form a planar tile structure for each complex.

The dimensions of the 4-, 8-, and 12-HT complexes are calculated to be  $\sim 17 \times 7 \times 3$ ,  $\sim 17 \times 14 \times 3$ , and  $\sim 17 \times 21 \times 3$  nm, respectively, assuming no inter-helical distance. If an inter-helical distance of  $\sim 1$  nm is assumed, the dimensions would be  $\sim 17 \times 10 \times 3$ ,  $\sim 17 \times 18 \times 3$ , and  $\sim 17 \times 27 \times 3$  nm, respectively. The anisotropy of dimensions in the  $x$ – $y$  plane for all three tiles is smaller than the DX tiles and minimized in the 8-HT tile. The DNA sequences of the 4-, 8-, and 12-HT complexes were designed with the program SEQUIN<sup>27</sup> to minimize the chance of sequence symmetry and presumably the probability of misfolding. The strand sequences for each

(26) Deng, Z.; Mao, C. *Angew. Chem., Int. Ed.* **2004**, *43*, 4068–4070.

(27) Seeman, N. C. *J. Biomol. Struct. Dyn.* **1990**, *8*, 573–581.

(28) Rodbard, D.; Chrambach, A. *Anal. Biochem.* **1971**, *40*, 95–134.

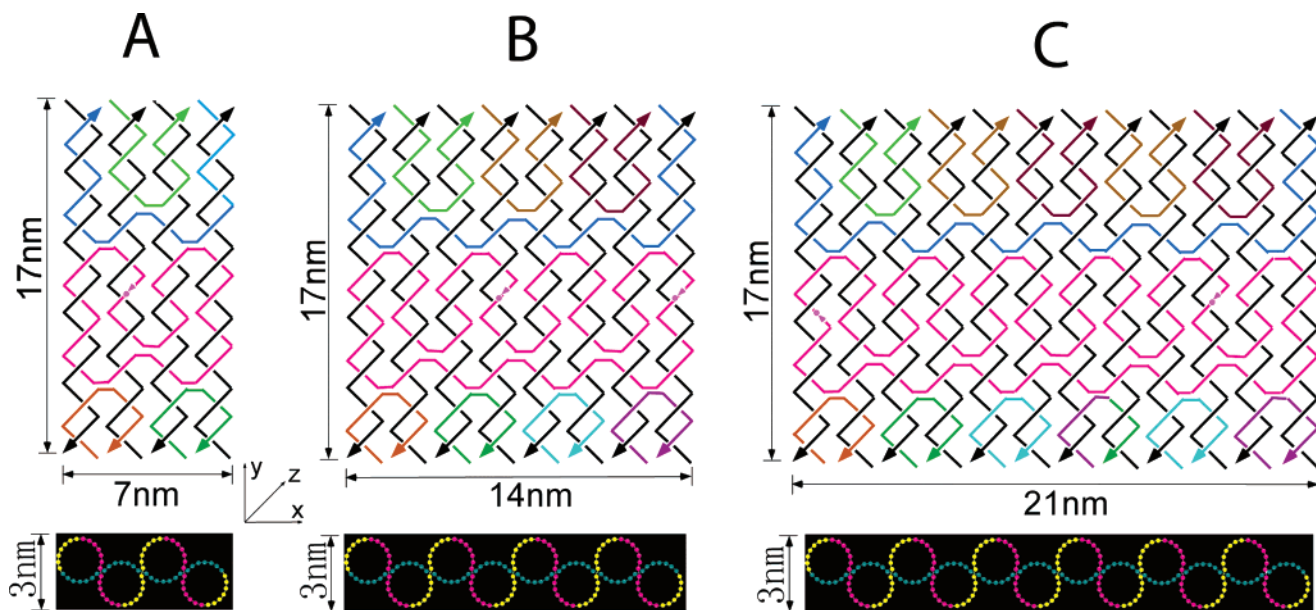


**Figure 1.** Design of 4-, 8-, 12-helix DNA nanostructures. (A) 4-Helix complex. This molecule can be viewed as two DAE molecules joined together by two DAE-type crossovers. Crossovers are staggered across the width of the tiles; each pair of crossovers between neighboring helices is shifted up or down 7 nucleotides with respect to adjacent pairs of crossovers. (B) 8-Helix complex. This complex extends the same design principle of the 4-helix complex with 4 more helices added to its side. (C) 12-Helix complex. This complex extends the same design principle of the 4-helix and 8-helix complexes. On the bottom are the views of the tiles along the *y* axis from the end of the helices. The *x*, *y*, and *z* dimensions of the tiles are labeled on the sides. The dots and arrows on the central pink colored strands indicate the 5' and 3' ends of the nick points.

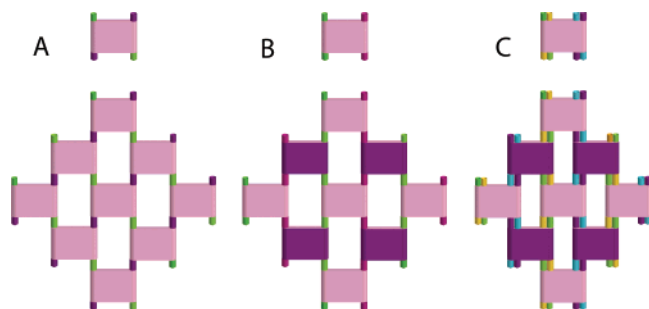


**Figure 2.** Schematic view of the three sticky end connection designs for the formation of 2D arrays from the rectangular tiles. (A) 1SE. (B) 1SE-C. (C) 2SE-C. The different colored short columns represent the sticky ends, and complementary sticky ends are shown in the same color. The light and the darker colored tiles indicate the tiles are facing in opposite directions to each other (in or out of the paper perpendicularly).

individual tile are given in the Supporting Information. The nick points for the central backbone strands are chosen to make an asymmetric break in the strand, so at least one of the strands can still wind through all of the helices.

Sticky ends are designed into the four corners of the tile to “glue” them into 2D arrays. Figure 2 illustrates the three different sticky end designs used for each tile system: (A) single helix sticky end connections with neighboring tiles all facing in the same direction (termed as 1SE), (B) single helix sticky end connections with neighboring tiles flipping 180° alternatively (corrugated design, termed as 1SE-C), and (C) two-helix sticky ends connections with corrugated design (termed as 2SE-C). To avoid nonspecific blunt end stacking between the tiles, the ends of the helices in the center of the tiles that do not carry the sticky ends are terminated with T<sub>4</sub> single-stranded fragments. The self-assembled lattice structures contain periodic cavities that can be easily visualized by AFM. The above designs allow us to examine the influences of the following factors that might

affect the formation of DNA tubes: different tile sizes, sticky end strength, and flexibility.

## Results and Discussion

**Assembly of the Tile Motifs.** Formation of specific molecular weight complexes by annealing stoichiometric mixtures of component strands was analyzed by nondenaturing PAGE. The gel image in Figure 3 demonstrates the formation of the 4-HT complex (without sticky ends). The single and distinct band in lane 9 corresponds to the complete formation of the 4-HT complex, indicating specific base-pairing to form an intact structure without significant unexpected intermolecular association or dissociation of the complex. The partial formations of the complex in lanes 2–7 were revealed as faster migrating bands as compared to the band containing the whole complex. Some of the partial complexes show multiple bands resulting from poor complementarity in the absence of properly matched partners. This is a common phenomenon for partial combinations of the strands. When all of the strands involved in the tile complex were annealed with perfect stoichiometry, no unwanted hybridization was evident on the gel. 8-HT and 12-HT used the same design principle as the 4-HT with extra helices extending in the tile plane, and their corresponding complexes were also shown as intact bands on nondenaturing gel (data not shown). The thermal stability of the tiles was also examined (data are shown in the Supporting Information). The 4-HT has two transitions, the most profound at  $\sim 58 \pm 7$  °C, and the second at  $\sim 65$  °C. The 8-HT and 12-HT complexes show single transitions that occur at  $\sim 65 \pm 5$  and  $\sim 62 \pm 8$  °C, respectively. Sharp transitions in the melting temperature measurements confirm the cooperativity of all of the component strands in the formation of individual tiles.

**Self-Assembly of the 4-HT, 8-HT, and 12-HT.** When sticky ends are added to the corners of the tiles, they guide the tiles to self-assemble into 2D arrays as coded in the sequence and

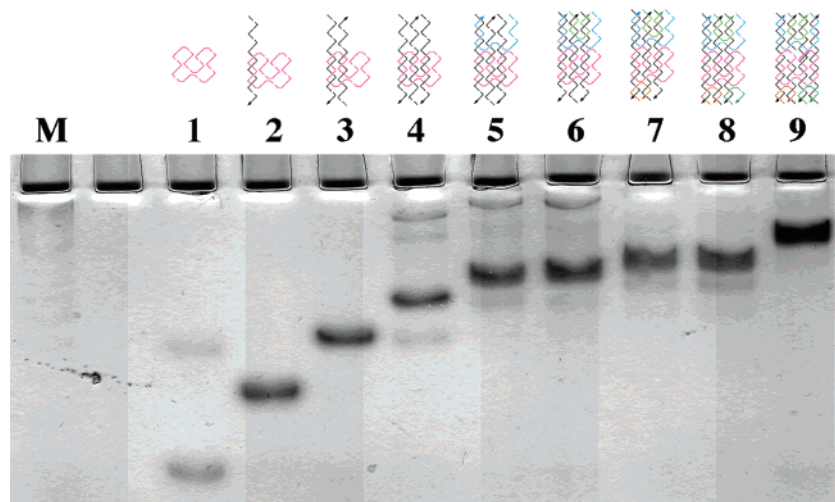


**Figure 3.** Nondenaturing gel (8% polyacrylamide) of the 4-helix complex stained with Stains-all. Equimolar mixtures of 1  $\mu$ M of each strand were annealed, and the electrophoresis was run at room temperature. Lane M is a 100 bp DNA ladder. Lanes 1–8 contain complexes with partial combination of the component strands. Strands included in the annealing are indicated with a schematic drawing above the lane. Lane 9 corresponds to the full complex with all of the component strands.

complementarity of the sticky ends. A gallery of AFM images is shown in Figure 4 with zoomed-in pictures clearly demonstrating the characteristics for the rectangular-shaped tiles, dimensions of the cavities for each tile, and connection design. For example, in the 1SE connection, the distance between the inter-tile crossover points is 2 full turns for the 4-HT tile, and 3 full turns for the 8-HT and 12-HT tiles. In the 1SE-C and 2SE-C connections, the distance between the intra-tile crossover points for all three tiles is 2.5 full turns; thus the length of the cavity in the self-assembled tile arrays should have the relations: for 4-HT,  $1SE < 1SE-C \approx 2SE-C$ , and for 8-HT and 12-HT,  $1SE > 1SE-C \approx 2SE-C$ . The widths of the cavities should have the following relationship:  $1SE \approx 1SE-C > 2SE-C$ . These relationships are verified from the zoomed-in images.

By design the 4-HT tile theoretically forms a  $\sim 4$  nm wide cavity for the 1SE and 1SE-C connectivity, and no cavity for the 2SE-C connectivity. The cavity size for the 1SE and 1SE-C can be seen, although this is close to the limit of the resolution of the AFM tip. For the 2SE-C connection, where no cavity is expected, the individual tiles in the images can still be clearly distinguished from each other. The triangle-shaped void spaces between the tiles reveal that the helices are all flexible, at least at the crossover points. For example, the 4-HT tiles in the 2SE-C connection may be considered as an “X”-shaped tile. This is true for all of the tiles. The shape deformation away from the rectangular shape is more obvious for 8-HT and 12-HT in the 1SE connection because of the longer arms (3 full turns). The shape deformation is relatively smaller for the 1SE-C and smallest for the 2SE-C because of the shorter arms (2.5 turns) and double strength of the sticky ends, respectively.

It is noted that the molecular weights of the 8-HT and 12-HT tile are 1000 and 1500 nucleotides, respectively, consisting in total of 18 and 27 single strands with lengths varying from 26 nucleotides to 130 nucleotides. The size of the tiles and number of strands per tile are 3–5 times larger than those commonly used in other studies.<sup>1,2</sup> All of the strands for one tile are mixed together in one tube and annealed. No purification of the lattice was performed. The concentration of each strand was measured carefully, and a standard deviation within 5% was ensured for all of the strands, limiting the number of tiles

with incomplete structure to less than 10%. The successful formation of these tiles proves that DNA tiles in this size range are plausible and represents a milestone in constructing DNA tile motifs. It is also possible that incomplete tiles missing some noncritical strands can still be incorporated into the lattices. We think the most important strands in each tile are the long strands (in pink and blue color in Figure 1) that weave through the entire helix because they link all strands into an integrated unit. As limited by synthesis capability, the longest strand ( $>200$  nt) in the 8-HT and 12-HT tiles is chopped into two shorter strands. We chose an asymmetric break to make sure that at least one of the strands can weave through all helices. The four strands with the sticky ends are also important for the tile to grow into the lattice. The absence of a few short strands along the edges of the tile would not affect a tile’s ability to bind into a growing lattice and would not inhibit further growth.

Table 1 summarizes the morphology of the self-assembled structures observed for the three tiles with the three different sticky end associations.

Large and flat 2D arrays are the dominant structures formed from the 8-HT tiles, although some tubes coexist for the 1SE and 2SE-C connections. For the 4-HT and 12-HT tiles, no matter what the connections are, the tiles always grow into tubes. The tubes formed from 12-HT tiles seem to open easily either immediately upon being deposited on the mica substrate or after the AFM tip is scanned over that area, as some debris from the top layer can still be observed. It appears that the lattices or tubes do not form as well when the number of helices is increased from 4 to 8 and 12 (and the number of strands per tile increases) as evidenced by a higher background in the AFM images. This might be due to an increased number of malformed tiles as the number of strands increased.

For the 8-HT tiles, in the 1SE connection, many tubes were observed, but in the 1SE-C connection, no tubes were observed. This difference can be explained by Rothmund et al.’s model for DAE-E tubes<sup>22</sup> based on the intrinsic angle between the neighboring tiles. When the tiles all face in the same direction, the angle accumulates over a layer of tiles and the tile array can wrap into a tube. Within this model, for the corrugated design (1SE-C and 2SE-C) there is no angle between the

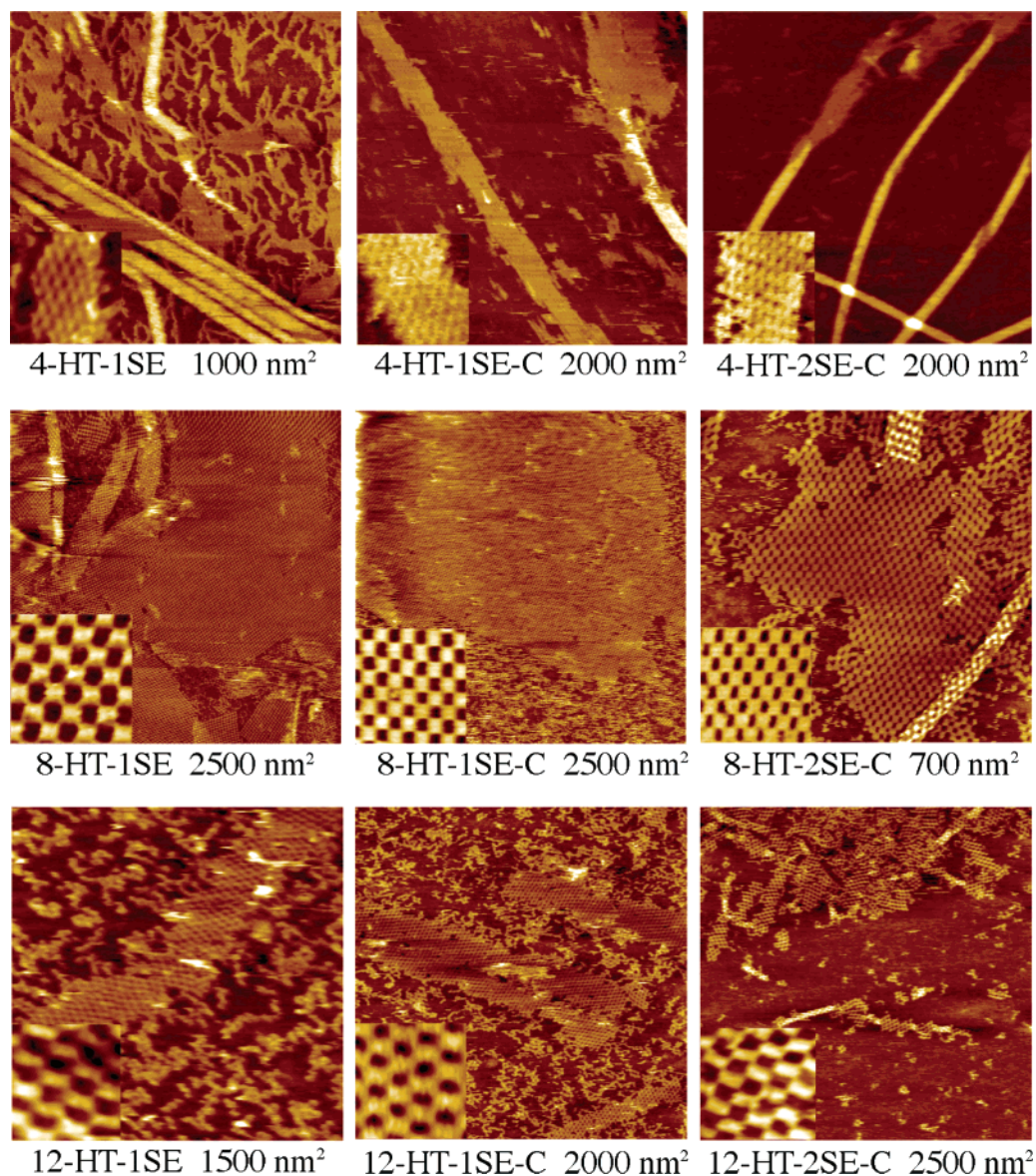


**Figure 4.** A gallery of the characteristic AFM images for the lattices self-assembled from 4-, 8-, and 12-helix DNA nanostructures using the three different sticky end connection strategies. Each AFM image contains a  $120 \times 120 \text{ nm}^2$  zoomed-in inset. The complex and connection strategy used and the scan size are labeled below each image.

**Table 1.** Observations for Self-Assembly of the 4-, 8-, and 12-Helix Tiles

	1SE	1SE-C	2SE-C
4-HT	tubes, narrow tube diameter distribution	tubes, wide tube diameter distribution, easily opened	tubes, narrow tube diameter distribution
8-HT	tubes and 2D arrays	2D array only, no tubes	tubes and 2D array
12-HT	tubes, narrow and easily opened	tubes, wide distribution of tube diameters, easily opened	tubes, narrow tube diameter distribution, easily opened

neighboring tiles, and thus no tube is expected. However, this model cannot explain the tubes found in this study in the case of 2SE-C.

Based on Turberfield and co-workers' model,<sup>24</sup> because tubes were observed for 8-HT tile with 2SE-C, one could conclude that the bond energy gain (for a double sticky end) was high enough to overcome the strain energy penalty (to twist two DNA helices simultaneously), so that tube formation was thermodynamically allowed. When the double sticky end is changed to the single sticky end in the 1SE-C, the bond energy gain per unit area is reduced by one-half. In this case, the strain energy penalty to twist one DNA double helix as compared to twisting two DNA double helices simultaneously would be reduced to

at least one-half. This implies that if tubes are observed in the case of 2SE-C, then tubes should also be observed for 1SE-C. Because no tubes were observed in the case of 1SE-C for the 8-HT tile, we think other factors must be involved.

We propose that tube formation is allowed thermodynamically for both 1SE-C and 2SE-C connections, but whether tubes really form is determined kinetically. This is supported by calculations<sup>24</sup> that by using the twisting modulus of a DNA double helix to mimic the bending modulus of the tile connection point, the minimum tube circumference in the 1SE-C could be as small as 6 times the width of the tile (without helicity). The bending modulus of the tile connection was so small that a tube with a 6-tile perimeter is allowed energetically.

**Table 2.** Maximum Length ( $\mu\text{m}$ ) of the Tubes Observed by AFM

	1SE	1SE-C	2SE-C
4-HT	11	10	20
8-HT	2		11
12-HT	3	9	1.4

**Table 3.** Average Widths (nm) of the Tubes (Measured from 10 Tubes for Each Case)

	1SE	1SE-C	2SE-C
4-HT	42 $\pm$ 13	82 $\pm$ 23	39 $\pm$ 4
8-HT	100 $\pm$ 50		86 $\pm$ 45
12-HT	55 $\pm$ 25	133 $\pm$ 39	43 $\pm$ 12

**Table 4.** Average Angles (deg) between Tube Axis and Tile Helix Axis (Measured from 10 Tubes for Each Case)

	1SE	1SE-C	2SE-C
4HT	0 $\pm$ 2	24 $\pm$ 1	20 $\pm$ 4
8HT	0 $\pm$ 4		13 $\pm$ 4
12HT	9 $\pm$ 4	35 $\pm$ 2	10 $\pm$ 5

The formation of a tile array can be roughly divided into two stages: nucleation and growth. Nucleation is the first step, beginning with two or three tiles hybridized together through sticky ends interactions. Growth includes addition of tiles to all sides of the array, resulting in a larger patch of array. Because of the anisotropic aspect ratio of the tile, the growth rate of the tile array in length is not equal in the two directions. The sticky ends at the four corners of the rectangular tiles are all of similar strength (if not exactly the same); they allow for similar rates of growth in terms of number of tiles that get attached per unit time. The resulting tile array will ideally have an equal number of units along both principal axes; thus the dimensions of the tile array would roughly keep the same aspect ratio of its unit. For example, the 4-HT has the aspect ratio of  $\sim 2$ , and the resulting tile array would also be narrower along the width of the tile. Along the width of the tile, the tile array also has less stiffness. If the array wraps up into a tube when it is still narrow enough, the growth in the width direction will stop and now can only occur at the ends of the tube, producing long narrow tubes. On the other hand, when the tile array is allowed to grow quickly to a size that exceeds its persistence length, the chance for the closing of the tube drops dramatically, and thus the array would continuously grow bigger.

8-HT tile has the minimized dimensional anisotropy, which leads to similar growth rates in both directions in terms of length per unit time. Large patches of tile arrays are formed for all of the connections, despite the fact that the tile is anisotropic in stiffness, that is, easier to bend around the axis parallel to the helical axis to form tubes. Certainly tubes sometimes coexist with large arrays. The tubes formed in the case of 1SE may be due to the presence of a curvature in the tile array so that there is less of an energy barrier for tube formation. The tubes observed in the case of 2SE-C may be due to a more negative bond energy so that there is higher driving force for tube formation.

Tables 2–4 list some of the measurements of the tube width, length, and angle from the AFM image analysis. Average tube width ( $W$ ) and angle ( $A$ ) were expressed as numerical means  $\pm$  (max – min)/2. Below are some interesting observations.

(1) Removal of curvature in the tile array can indeed hinder tube formation because tubes formed with a curvature are generally narrower than the tubes formed without a curvature. This is evident by comparing the 1SE and 1SE-C. For 8-HT, tubes can be found in the 1SE, but no tube was observed in the 1SE-C. For 4-HT and 12-HT, the 1SE-C produced tubes wider than the 1SE. However, the presence of an intrinsic curvature does not guarantee that the tile array would form tubes exclusively. This is evidenced by the AFM images for 8-HT-1SE and worth noting. This indicates that the aspect ratio of tiles plays a greater role in tube versus sheet determination.

(2) For the same tile, the stronger is the connection, the more tendency there is to form tubes. This is evident by comparing 1SE-C and 2SE-C. The 2SE-C connection leads to tubes for all of the tiles, and the tubes are narrower than the 1SE-C.

(3) For the same connection, the more anisotropic and flexible are the tiles, the greater tendency there is to form tubes. Comparing 4-HT, 8-HT, and 12-HT, 4-HT is most anisotropic, and 12-HT is most flexible (less stiff) along the direction perpendicular to the helical axis in the tile plane. Therefore, 4-HT and 12-HT have more tendency to form tubes than 8-HT. The tube width has the following trend: 4-HT < 12-HT < 8-HT. This is clearly evident from the AFM analysis.

(4) The tubes can have a certain helicity. In addition to the twisting motion around the helical axis, the arms with the sticky ends can have two more angular motions with respect to the crossover points: rotating around the tile axis out of the tile plane and bending away from the tile axis within the tile plane. Because of these flexibilities, the energy barriers to wrap a patch of tiles in different directions are close. Therefore, tubes with different circumferences and helicities can form. Figure 5 illustrates the formation of the helicity of the tubes and zoomed-in images of the tubes formed. Upon wrapping of the 2D array into tubes, the connection of the tiles from one end to the opposite side of the array can be offset by an integral number of rows as shown in case 1 or without offset as shown in case 2. The angle  $\theta$  between the tube axis and the tile helix axis can be calculated by  $\sin \theta = nl/mw$ , where  $n$  is the number of rows of the offset,  $m$  is the number of tiles in one row to form a whole wrap,  $l$  is the repeating unit of the length, and  $w$  is the repeating unit of the width. For example, in the case of 12-HT tile in the 2SE-C connection, a tube width is measured as 42 nm (when it is pressed on the flat surface of the substrate), representing only 4 tiles to close a complete wrap. Using the measured angle  $\sim 10^\circ$  and the dimensions of the tile, we can calculate that this tube has one row of tiles offset. The angle between the tile axis and the tube axis is close to zero for the 1SE connection, the tube formation of which is dominantly driven by the intrinsic curvature, and the tubes are narrow, involving 7–15 tiles to complete a whole perimeter. For the 1SE-C connections, the angle between the tube axis and the tile axis is in the range of 24–35°. In this case, the tube formation is not limited by steric restrictions as is the case in 1SE; therefore, the tubes are wider and with wider distribution, involving a range of 10–20 tiles to complete a whole perimeter, and the connection of the tiles across the opposite ends of the 2D array can offset multiple rows of tiles, and thus the observed angles are larger. The 2SE-C is a stronger connection that favors tube formation. As a result, the tubes in 2SE-C are both narrower and have smaller angles with respect to the tile axis, in

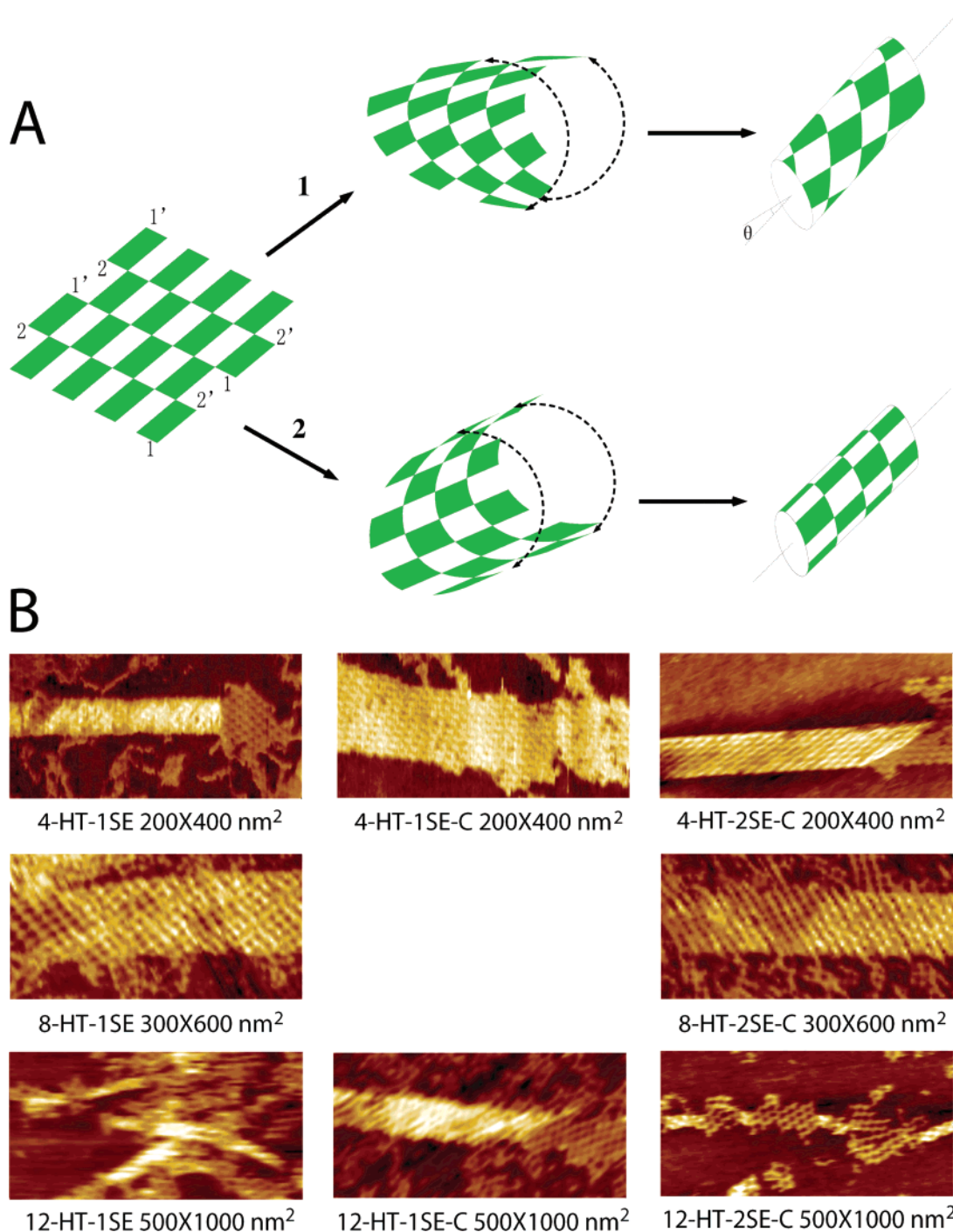


**Figure 5.** (A) Schematics showing the formation of the helicity of the tubes. Route 1: offset by 1 layer of tiles in the wrapping up of the tube. The tile axis has an angle with the tube axis. Route 2: no offset between the layers of the tiles in the wrapping up of the tube. The tile axis is parallel to the tube axis. (B) Samples of AFM images of the tubes revealing different helicities.

comparison to the 1SE-C for all of the tiles. The experimental results are consistent with our explanations about the tube formation.

### Conclusions

We have designed and characterized a new family of DNA tiles containing multiple helices. This group of DNA tiles not only provides new building blocks for nanoconstruction, but they also help us to gain more insight into the formation of tube-like structures self-assembled from these tiles. By investigating the effects of the tile dimension variables, we have

observed that the dimensional anisotropy of a DNA tile plays an interesting role in the DNA self-assembly process. Other parameters affecting the self-assembly of DNA tiles into tube structures include orientation of the tiles, flexibility of the tiles, and strength and flexibility of the connection points. Reduced tile anisotropy and rigid tile structure plus corrugated orientation can help the 2D lattice grow. There are surely other parameters involved but not tested here.

**Acknowledgment.** We thank Dr. Paul W. K. Rothmund for helpful discussions, the Bidesign Institute at ASU and the NSF

for financial support, and Kyle Lund and Berea Williams for help in proofreading the manuscript.

**Supporting Information Available:** Experimental methods used, DNA tile sequences, and results from the Ferguson

analysis and thermal profiles. This material is available free of charge via the Internet at <http://pubs.acs.org>.

JA058145Z